



HAL
open science

Analysis of a thermal correction method for infrared spectroscopy: preparation for the future observations of the Martian moons Phobos and Deimos with the MIRS instrument

Gaël David, Marco Delbo, Maria Antonietta Barucci, Frédéric Merlin, Abigail A. Fraeman, Sonia Fornasier, Giovanni Poggiali, Pierre Beck, Cédric Leyrat

► To cite this version:

Gaël David, Marco Delbo, Maria Antonietta Barucci, Frédéric Merlin, Abigail A. Fraeman, et al.. Analysis of a thermal correction method for infrared spectroscopy: preparation for the future observations of the Martian moons Phobos and Deimos with the MIRS instrument. Monthly Notices of the Royal Astronomical Society, 2024, 534, pp.3265-3276. 10.1093/mnras/stae2204 . insu-04836779

HAL Id: insu-04836779

<https://insu.hal.science/insu-04836779v1>

Submitted on 15 Dec 2024

HAL is a multi-disciplinary open access archive for the deposit and dissemination of scientific research documents, whether they are published or not. The documents may come from teaching and research institutions in France or abroad, or from public or private research centers.

L'archive ouverte pluridisciplinaire **HAL**, est destinée au dépôt et à la diffusion de documents scientifiques de niveau recherche, publiés ou non, émanant des établissements d'enseignement et de recherche français ou étrangers, des laboratoires publics ou privés.



Distributed under a Creative Commons Attribution 4.0 International License

Analysis of a thermal correction method for infrared spectroscopy: preparation for the future observations of the Martian moons Phobos and Deimos with the MIRS instrument

Gaël David ¹, ¹★ Marco Delbo,^{2,3} Maria Antonietta Barucci ¹, Frédéric Merlin,¹ Abigail. A. Fraeman,⁴ Sonia Fornasier ¹, Giovanni Poggiali ¹, Pierre Beck⁵ and Cédric Leyrat¹

¹LESIA, Observatoire de Paris, Université Paris Cité, Université PSL, Sorbonne Université, CNRS, 5 place Jules Janssen, F-92190 Meudon, France

²Laboratoire Lagrange, Observatoire de la Côte d'Azur, CNRS, Université Côte d'Azur, Nice, CS 34229, France

³School of Physics and Astronomy, University of Leicester, University Road, LE1 7RH Leicester, UK

⁴Jet Propulsion Laboratory, California Institute of Technology, Pasadena, CA 91109, USA

⁵CNRS, Université Grenoble Alpes, IPAG, F-38000 Grenoble, France

Accepted 2024 September 18. Received 2024 August 17; in original form 2024 February 9

ABSTRACT

The MIRS (MMX InfraRed Spectrometer) infrared spectrometer is part of the scientific payload of JAXA's (Japanese Space Agency) Martian Moon eXploration (MMX) mission. From the reflected sunlight by the planetary surfaces, MIRS will provide information on the Mars atmosphere and the mineralogy and chemistry of its moons. Spectra carried out by the instrument (0.9–3.6 μm) include the thermal emission from the surface, which needs to be modelled and removed to extract the compositional information. In this study, to find an efficient and rapid way to thermally correct infrared data, we developed a simple thermal emission correction based on blackbody fits, and quantify its relative error. To test the method, we generated synthetic spectra of Phobos by using a thermophysical model. We found that the method can produce reflectance spectra with only a few per cent errors, although some undercorrection of the thermal contribution is observed. Compositional information may still be retrieved through the position of absorption bands, despite the thermal emission correction can leave some uncertainties in its strength. We conclude that the method could be used for a first and quick analysis for interpretation of the MIRS data. We also applied our thermal correction methodology to real CRISM (Compact Reconnaissance Imaging Spectrometer for Mars) observations of Phobos. The method looks reliable with a satisfactory removal of the thermal contribution, confirms the presence of an absorption band centred around 2.8 μm , and reveals an apparent absorption at 3.2 μm . However, we are not able to confirm the reality of the 3.2 μm band at this stage, because of the presence of an artefact in CRISM data.

Key words: radiation mechanisms: thermal – space vehicles: instruments – techniques: imaging spectroscopy – planets and satellites: composition – planets and satellites: surfaces.

1 INTRODUCTION

The Martian Moon eXploration (MMX) is a sample return mission from the Japanese Space Agency (JAXA) (Kuramoto et al. 2022), scheduled to be originally launched towards the Martian system in 2024 but was recently postponed to 2026. MMX will study the Martian atmosphere, characterize the surface of the Martian satellites Phobos and Deimos using remote sensing observations, delivering a rover to interact with the surface of Phobos and returning Phobos sample to Earth. One of the major scientific goals of MMX is to constrain the origin of these moons. Indeed, there is not yet consensus in the planetary science community about their formation process. Two main hypotheses have been put forward that involve the capture by Mars of two asteroid-like bodies (e.g. Hartmann 1990; Higuchi & Ida 2017) or the accretion of debris produced by a giant impact

on Mars (e.g. Rosenblatt et al. 2016; Hesselbrock & Minton 2017; Hyodo et al. 2018). However, none of these hypotheses fully explain the observations, and each one has its own advantages and limitations. In particular, the spectral properties of Phobos and Deimos (and references therein, Poggiali et al. 2022) strongly differ from those of the surface of Mars, which may suggest that the planet and the moons have distinct origins. The two satellites are characterized by a low albedo and red spectra (i.e. reflectance increases with wavelength). Two different spectral units were determined on Phobos (e.g. Murchie & Erard 1996; Rivkin et al. 2002). The red unit is characterized by a spectrally red-sloped and covers most of the Phobos surface. To a lesser extent, a blue unit with a less red-sloped is also present on this moon. It is mostly associated within and around impact craters such as Stickney and then could correspond to deeper and excavated materials (Murchie et al. 1991). The cause of such spectral differences between the two units is not fully understood and several factors can contribute to the slope variation in near-

* E-mail: Gael.David@obspm.fr

infrared (NIR) spectra including composition and grain size and/or porosity of the regolith, as well as space weathering that can induce spectral changes (e.g. Takir et al. 2022). The spectral properties of the surface of Deimos are similar to those of the red unit that dominates the surface of Phobos. In both moons, no strong absorption is observed except the presence of weak ones at 0.65 and 2.8 μm (Fraeman et al. 2012, 2014). These spectral properties are more akin to primitive D- and T-type asteroids, Jupiter’s Trojan asteroids, or ultrared trans-Neptunian objects (e.g. Rivkin et al. 2002; Takir et al. 2022). Furthermore, the low density of Phobos and Deimos with respectively ~ 1.86 and ~ 1.48 g cm^{-3} (Jacobson 2010; Willner, Shi & Oberst 2014) are globally consistent with those of Jupiter Trojans, Trans-Neptunian objects, and D- and T-type asteroids (e.g. Stansberry et al. 2012; Marchis et al. 2012; Brown et al. 2021; Li et al. 2023). It has been proposed, based on these arguments, that Phobos and Deimos are objects originating from the outer part of the asteroid main belt or from the outer part of the Solar system that Mars could capture somehow. However, this scenario does not explain the quasi-circular and quasi-equatorial orbits of the two satellites (Rosenblatt 2011). On the other hand, the impact scenario has received growing attention in recent years (Craddock 2011; Rosenblatt & Charnoz 2012; Ronnet et al. 2016). It suggests that the collision between a young Mars and a large planetesimal (or planetary embryo) could have led to the formation of a circumplanetary disc, from which disc particles re-accumulated to form gravitational agglomerates, which are at the origin of the two moons that we observe today. This hypothesis explains the orbital properties of Phobos and Deimos, which have low eccentricities and inclinations compared to the equatorial plane of Mars. It has been commonly suggested that, in this scenario, the surface of Mars and its moons should have a similar composition. But this is not what appears from visible and IR spectroscopic observations, due to the extreme diversity of the spectrum of Mars compared to those of its moons. Nevertheless, a recent work suggested that the accretion of small (≤ 2 μm) dust particles resulting from impact-generated gaseous disc could explain the similarity in spectral properties between D-type asteroids (or comets) and the Martian moons, as well as their low densities (Ronnet et al. 2016).

To bring new constraints and help to determine which of the two scenarios mentioned above is the most appropriate, it is essential to finely constrain the mineralogical and chemical compositions of the surface of the two satellites at high spatial resolution. Indeed, the geological records of the moons may contain clues to their formation processes and evolution. MMX’s payload includes the MMX InfraRed Spectrometer (MIRS), a hyperspectral imaging spectrometer operating in the 0.9–3.6 μm spectral range, with a spectral resolution better than 20 nm and able to provide a signal-to-noise ratio (SNR) higher than 100 (Barucci et al. 2021). MIRS is specifically designed to characterize the materials making up the surface of the moons, in order to study their characteristics, distribution, and spatial relationships in relation to topography. Because of their different spectral properties, analysis of MIRS data can allow us to disentangle different phases of geological interest, such as hydrated and anhydrous silicate minerals (respectively with bands in the 0.9–1/2.0 μm regions and with features at 2.7–2.8 μm), water ice (absorption bands at 1.5, 2.0, and 3.0 μm) and organic matter (3.2–3.5 μm). MIRS observations will have a spatial resolution so far never reached at the surface of Phobos and Deimos, equivalent to 20 and 100 m, respectively. By providing constraints either in favour of the capture or impact scenario, MIRS observations will help to better constrain the processes of planetary formation and material transport in the regions connecting the inner and outer Solar systems. In the

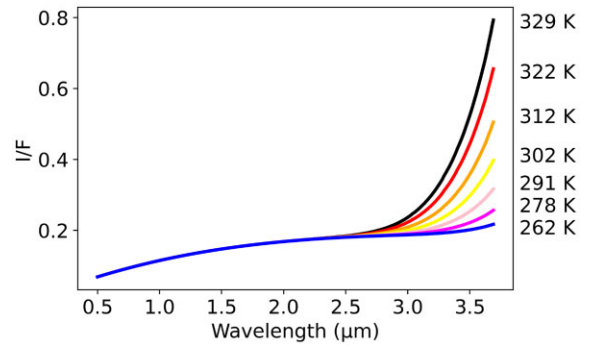


Figure 1. Synthetic spectra of Phobos generated using a thermophysical model (Delbo et al. 2015) showing the effect of the thermal emission for different surface temperatures. For wavelengths higher than ~ 2.5 μm and for high temperatures, this contribution is dominant compared to the reflected solar fraction.

case of Phobos, MIRS analyses will also be essential for selecting the two sample collection sites. During the sample-site selection process, MIRS will enable us to acquire surface mineralogical information at very high spatial resolution, that is, ~ 1 m, over about a 50 m radius around the sites under investigation. Thus MIRS will provide a link between the remote large-scale analysis of the moons, and the finely characterized samples brought back to Earth.

Before proceeding to the mineralogical/compositional analysis of MIRS data, several steps of calibration are needed. One of these steps includes thermal emission correction. This is because, in the IR spectral range, at wavelengths $\gtrsim 2.5$ μm , the signal collected by the instrument is a combination of reflected sunlight and thermal emission from the observed surfaces. This thermal emission strongly modifies the continuum of the spectra (e.g. Fig. 1) and the shape and intensity of the absorption bands if any are present in the affected wavelength range. The thermal emission correction is a crucial step for rigorous data interpretation, and in particular for studying the metal-OH absorption at 2.8 μm detected by Fraeman et al. (2014), as well as putative absorptions linked to water ice and organic matter. The thermal emission is mainly controlled by the surface temperatures and emissivities (ϵ) that are often not well constrained on planetary surfaces. For airless bodies, like Phobos and Deimos, the surface temperatures can be highly fluctuating, from ~ 150 up to ~ 350 K (Lynch et al. 2007; Giuranna et al. 2011), mainly due to the time-varying heliocentric distance, combined with the illumination variations generated by the diurnal and seasonal cycles. The thermal inertia of the surface’s materials also can strongly influence the temperatures and its diurnal variations (Delbo et al. 2015). Moreover, the thermal signal reaching MIRS is due to a combination of the emission of different surface elements, which have different temperatures. The rougher the surface, the stronger are in principle the temperature differences between elements within the MIRS pixel footprint. It is therefore evident that surface roughness plays a crucial role in the thermal emission of the surface.

Ideally, independent measurements of surface temperature acquired at the same locations and local times as IR spectra could be used to estimate and then separate thermal emission from surface reflectance. However, such data are unfortunately often not available. To remove the thermal contribution from the surface of planetary bodies, different approaches have been used in the past. For example, DellaGiustina et al. (2019) computed the temperature distribution at the surface of Bennu by means of a thermophysical model that takes into account several input parameters

(e.g. shape model, bond albedo, emissivity or thermal inertia) to correct the OSIRIS-REx (Origins-Spectral Interpretation-Resource Identification-Security-Regolith Explorer) visible and Infrared Spectrometer (OVIRS). The modelled flux is then computed from the model temperatures by summing the *Planck* function across facets in the OVIRS footprint. Hamilton et al. (2019) tried another method to correct OVIRS data, which used a smooth-surface thermophysical model assuming a spherical asteroid and that the spectrum of Bennu is flat from 2.2 to 4.0 μm . The reflected radiance was computed considering a subtraction of the model thermal radiance from the total measured radiance. In the work of Simon et al. (2020), for each spectrum, a linear continuum model was fitted from 1 to 4 μm with a slope of $0.05 \mu\text{m}^{-1}$, multiplied by a range-corrected solar spectrum, and scaled to Bennu's radiance at $-2.1 \mu\text{m}$. This scaled solar radiance is subtracted from the OVIRS spectrum to find the remaining thermal radiance. The thermal radiance spectrum is finally fitted with a single temperature blackbody curve by computing the blackbody radiance every 1 K from 150 to 475 K, scaling to the measured thermal radiance. For Moon Mineralogy Mapper (M^3) data, Clark et al. (2011) performed an extrapolation of the apparent lunar reflectance of the spectral continuum in a region not affected by thermal emission beyond 2.5 μm . Temperatures are then estimated using the *Planck* function at a given wavelength along with a reflectance and emissivity thanks to Kirchhoff's law ($r_{(\lambda)} = 1 - \varepsilon_{(\lambda)}$). On the same data, Li & Milliken (2016) developed a similar empirical model but based on a power law between the reflectance at 1.55 and 2.54 μm , empirically observed in laboratory reflectance spectra of Apollo and Luna soil and glass-rich samples. Radiance at 2.54 μm that is in excess of the expected amount is assumed to be due to thermal emission and is removed. Unlike previous approaches that require extrapolation of the spectral continuum in the thermal region, Raponi et al. (2019) model for Ceres observations the solar-reflected radiance (solar spectrum scaled to the heliocentric distance and modelled by a photometric function in such a way that the surface topography and/or the photometric characteristics of the surface can be taken into account) and the thermal emission by the product of *Planck* function and effective emissivity. Once the thermal emission has been derived, it is subtracted from the total measured radiance. On the asteroids Vesta and Lutetia, Coradini et al. (2011) and Tosi et al. (2014) used a Bayesian approach to nonlinear inversion to calculate surface temperature. In this method, surface spectral reflectance is also modelled by photometric functions that require good knowledge of the observational geometry achieved by means of a shape model. Then, the pair of unknown parameters (i.e. spectral emissivity and temperature) providing the best fit with the measured spectral radiance are iteratively and simultaneously computed until convergence around stable values is achieved. Finally, Fraeman et al. (2014) used a hybrid approach to the thermal modelling of CRISM observations. They first used the method of Clark et al. (2011) correction to estimate what a reasonable surface temperature should be. Then, they used the temperature value with the full Hapke (1993, 2012) model along with the radiance from CRISM to solve for single scattering albedo.

In this study, we developed and tested a method for the correction of the thermal emission for the IR data that will be obtained by means of MIRS. We present a relatively simple method of thermal emission correction that can be easily implemented in the MIRS data reduction and calibration pipeline. The method does not require a priori information about the surface being observed, in contrast to more sophisticated methods of predicting the thermal emission based on thermophysical models. We deliberately explored a simple empirical method, based on blackbody function fits to the region of

the spectrum containing the thermal emission contamination. This is also because the MIRS instrument will provide a large amount of data and a method running quickly will save computing time and make it easier the data interpretation during MMX flight operations, in particular, will be crucial for the sample site selection.

The method of thermal emission correction is first applied to synthetic data, within which the thermal contribution is fully modelled and therefore known. These data are generated for this study by means of a thermophysical model (Delbo et al. 2015), in which parameters have been given values representative of Phobos surface, illumination, and observing conditions. From these synthetic data, we quantify the relative error of the method for all wavelengths of the spectra generated. The aim is to determine how the error can evolve as a function of the thermal contribution, but also as a function of wavelength for a given spectrum. Additionally, we simulated the presence of an absorption band in the emission-contaminated part of spectra, in order to constrain the reliability of the method for estimating the band depth after thermal correction. For an application to MIRS observations (and for any IR data using this method), these results will be important as they will provide guidelines for interpreting the data. In the second step, the thermal correction method is applied to real Phobos observations that were obtained by the CRISM imaging spectrometer onboard the Mars Reconnaissance Orbiter spacecraft, with the aim of seeing how the model behaves on real data from Phobos.

2 METHODS

2.1 Thermal emission correction

In the approximation that the emissivity is independent of the incident and emission angles and spatially homogeneous within the instrument footprint, the radiance (intensity), $I_{(\lambda)}$, collected by an IR spectrometer can be expressed as:

$$I_{(\lambda)} = r_{(\lambda)}J_{(\lambda)} + \varepsilon_{(\lambda)}B_{(\lambda,T)}, \quad (1)$$

where λ is the wavelength, $r_{(\lambda)}$ is the reflectance, $J_{(\lambda)}$ is the solar irradiance at the heliocentric distance of the object's surface, $\varepsilon_{(\lambda)}$ is the emissivity of the surface, and B is the thermal emission (Hapke 1993, 2012). The latter can be approximated as:

$$B_{(\lambda,T)} = \int P_{(\lambda,T)}dA_{(T)}, \quad (2)$$

where $P_{(\lambda,T)}$ is the *Planck* blackbody radiation of a surface element dA at a temperature T , projected on the plane orthogonal to the line of sight. The surface integral is performed on the instrument footprint. The inverse method that shall be used in this work, from Clark et al. (2011) makes the assumption that $B_{(\lambda)}$ can be approximated by a single blackbody $B'_{(\lambda,T')}$ radiation with an effective temperature T' , the latter being determined from the data of each observation. $B'_{(\lambda,T')}$ can be expressed with the *Planck* function as:

$$B'_{(\lambda,T')} = \frac{2hc^2}{\lambda^5} \frac{1}{e^{\frac{hc}{\lambda kT'}} - 1}, \quad (3)$$

where h is *Planck's* constant, c is speed of light, and k is Boltzmann constant.

The method used in this study consists of determining the effective temperature and emissivity from spectra themselves and model the thermal emission contribution to total radiance $I_{(\lambda)}$ in order to retrieve the signal of the reflected solar radiance. We used the approach developed by Clark et al. (2011) that was originally developed to correct the Moon Mineralogy Mapper (M^3) observations onboard the

Chandrayaan-1 spacecraft, and was used in the calibration pipeline of said instrument. This method has been shown to be effective in correcting the lunar reflectance data up to about $3.3 \mu\text{m}$ (M^3 maximum wavelength). This approach is an iterative method and uses the assumption that the continuum of the reflected solar component is approximately linear beyond $2.5 \mu\text{m}$. The signal at shorter wavelengths (where the thermal contribution can be assumed negligible for Phobos and Deimos surface temperatures) is used to extrapolate the reflected contribution to longer wavelength in the part of the spectrum where the thermal emission becomes important. The differences between the extrapolated reflectance and the measured spectra are assumed to be due to the thermal contribution. The temperature T' of equation (3) multiplied by the emissivity and varied until the best fit for modelled the thermal emission contribution is obtained, therefore deriving the value of the effective temperature. The method begins by estimating the emissivity and the thermal contribution in the region $\geq 2.5 \mu\text{m}$ by extrapolating of the reflectance deduced from the intensity at $\leq 2.5 \mu\text{m}$ as in Clark et al. (2011). Given an estimate of the thermal contribution, this is removed from the $I_{(\lambda)}$ to obtain a new estimation of the reflected solar radiance contribution only in the region affected by the thermal emission. Hence, a new iteration can be performed. This method performs up to three iterations to adjust the temperature, using each time the previously corrected spectrum. While in the first iteration, emissivity is considered as constant with wavelength, the second and third iterations will consider a wavelength-dependent emissivity (i.e. Kirchhoff's law is used for each wavelength), in addition to an incidence angle correction (i.e. by dividing reflectance obtained by the cosine of solar incidence angle). If the temperature retrieval of the first and second iterations is within 1 K, then the third iteration is not performed. More details about the method can be found in Clark et al. (2011).

The complexity to set up this model lies in the choice of the wavelengths that will be used for extrapolations. These wavelengths must not be affected by the presence of absorption bands. For the first iteration, a linear fit is performed between 2.1 and $2.3 \mu\text{m}$ and then extrapolated to $3.5 \mu\text{m}$. For the second and third iterations, the wavelengths at 2.6 and $2.9 \mu\text{m}$ are used as anchors to extrapolate the reflected light component.

2.2 Simulation of thermal emission and reflected spectra

First, the model for the thermal emission correction of MIRS data, which is described in the previous section, was tested on simulations of the intensity (radiance) that MIRS would measure from the surface element of Phobos, following equation (15.31) of Hapke (1993, 2012), which has two components: reflected and thermally emitted. The component of the radiance from the reflected light was calculated by multiplying the bidirectional reflectance by the solar irradiance (Kurucz 1993). We used Hapke's photometric function (Hapke & Wells 1981; Hapke 1984, 1986; Mermy et al. 2023) to calculate the bidirectional reflectance considering the incident, emission, and phase angle, and depending on the so-called Hapke's parameters, which are the single-scattering albedo ω , the opposition surge width h , the opposition surge amplitude B_0 , the single-particle phase function parameter g , and the average slope of macroscopic roughness $\bar{\theta}$. These parameters were set to the respective values of 0.075 , -0.250 , 0.059 , and 2.53 , while two cases were considered for $\bar{\theta}$, namely a rough surface with $\bar{\theta} = 39^\circ$ and a smooth surface with $\bar{\theta} = 0^\circ$. The bidirectional reflectance was calculated at $0.55 \mu\text{m}$ and then multiplied by a normalized spectrum that we selected as representative the red unit of Phobos. We considered spectra from Rivkin et al. (2002), Fraeman et al. (2014), and Takir et al.

(2022). The thermal radiance was simulated using a thermophysical model (Delbo et al. 2015), which calculates thermal IR spectra of airless bodies, or subportions thereof, as a function of several physical parameters such as albedo, roughness, thermal inertia, rotation period, direction of the rotation axis, as well as illumination and viewing geometry. For non-zero thermal inertia, the temperature history of the facets of the body and their subsurface must be taken into account. This is achieved by starting the simulations 20 rotations of Phobos before the epoch of the radiance calculation. The surface of the body within the instrument footprint (e.g. pixel) is simulated as a mesh of triangular facets. View factors between the facets may be taken into account to simulate mutual heating and shadows. However, in the cases simulated here, the view factors are equal to zero as we always consider convex surfaces. More details about the thermophysical model can be found in Delbo et al. (2015). To keep consistency between the reflected and thermal components of the radiance, we adopted the method described by Āurech et al. (2017) in order to calculate the bolometric Bond albedo, which was expressed in terms of the wavelength-dependent reflectance. In addition, the model thermal radiance is multiplied by the directional emissivity ε , which was calculated using Hapke's formalism (i.e. equation 15.20 of Hapke 2012) from knowledge of the albedo factor and emission angle. The former is expressed in terms of the Hapke's parameters mentioned above (Hapke 2012). For all simulations ε resulted between 0.964 and 0.987 , depending on the wavelength.

Four different spectral data sets were generated, with the technique above, namely: (1) a first data set consisting of seven synthetic spectra (from 0.5 to $3.69 \mu\text{m}$) for which the thermal emission contribution was calculated at different temperatures from 262 to 329 K (Fig. 1); roughness was not modelled and the scene corresponded to a flat facet in nadir view. The model thermal inertia was varied between a few and few thousands $\text{J m}^{-1} \text{s}^{-0.5} \text{K}^{-1}$ in order to obtain different surface temperatures, and (2) in a second data set, the same physical parameters were used, but this time, the effect of roughness was generated by adding hemispherical section craters, with 90° semi-opening angle and 0.5 areal density on the facet (e.g. Delbo, Cellino & Tedesco 2007). This can be calculated to correspond to a $\bar{\theta}$ of 39° . Hence, the value announced before. This means that subfacets with different inclinations with respect to the sun and the instrument, namely those inside craters, compose the field of view. Each subfacet contributes to the thermal IR flux with its own temperature, which depends on the geometry relative to the sun, shadowing, and mutual heating (Delbo et al. 2007, 2015); (3) in a third data set, we generated seven spectra that included synthetic absorption band centred at $3.2 \mu\text{m}$ (mimicking the presence of organic species), to study its effect on thermal emission correction, and our ability to retrieve the band after the correction; while in the three previous simulations, the solar incidence angle θ has been set to zero, and (4) in a fourth simulation that also includes a fake absorption band, we varied θ between 0° , 20° , 40° , and 80° . Finally, from these four data sets, 50 spectra are then generated for each 'clean' spectrum by adding a Gaussian noise, with an SNR of 100 to approach the data that will be acquired by the MIRS instrument on Phobos, in order to study the influence of the noise in the thermal correction results. This is achieved by using the probability density function of the normal distribution to draw random samples at each wavelength of the spectra.

To determine the error of the thermal emission correction, we quantified the difference between each corrected spectrum and its spectrum of reference (i.e. spectrum generated without thermal emission contribution), by using the absolute percentage error (APE)

that can be expressed as :

$$\text{APE} = \left| \frac{r_{y(\lambda)} - r_{x(\lambda)}}{r_{y(\lambda)}} \right| \times 100, \quad (4)$$

where $r_{y(\lambda)}$ and $r_{x(\lambda)}$ are *I/F* values of the reference and corrected spectra for each wavelength in the thermal part (i.e. $\lambda > 2.5 \mu\text{m}$).

2.3 Application to real data from CRISM

To test the thermal correction method on real data, we used the Phobos observations obtained by the CRISM imaging spectrometer onboard the *Mars Reconnaissance Orbiter* spacecraft. These data have a comparable spectral range and spectral resolution than those that will be provided by the MIRS instrument. We used IR spectra (L-detector) from the CRISM cube FRT00002992.03 acquired on 2007 October 23 with a spatial sampling of 350 m pixel^{-1} . The incidence angles used in the second iteration of the thermal correction model were obtained from the work of Fraeman et al. (2014), and were calculated using P. Thomas' shape model and the SciBox toolkit (Thomas 1993; Choo et al. 2014). Among all the spectra of the CRISM cube images, we selected two groups of spectra corresponding to the two spectral units observed on Phobos: the red and blue units. Twelve spectra of the red unit were selected, as well as 12 spectra of the blue unit. Selected spectra correspond to adjacent pixels in both selection (3×4 boxes), with similar geometric conditions. Each spectrum has been individually thermally corrected.

3 RESULTS

3.1 Thermal emission correction on simulated spectra

In the first set of data generated by the thermophysical model, since a single planar facet is modelled, a unique temperature is included in the scene simulated for MIRS. Hence, it is possible to directly compare the temperatures of the blackbody obtained by our thermal emission correction method, T' , with the simulated facet temperature, T . For the first iteration of the model, we found that the spectrum with the low thermal emission, the temperature estimate is the worst. At $T = 262 \text{ K}$, we observed a divergence of 148.9° from the true temperature T (Fig. 2). However, the temperature prediction improves with increasing thermal contribution in the data. From $T = 302 \text{ K}$ and for higher temperatures, we found an error of less than 0.78 K with the true value. While the temperature predicted by the first iteration is not accurate at low thermal contributions, the second and third iterations give much better results for every temperatures. At $T = 262 \text{ K}$, we found a divergence of only 6.6° and 5.2° , respectively, and the prediction also improves with increasing surface temperatures. From $T = 278$ and up to 329 K , we found an average of absolute difference between T' and T over the six spectra of $|T' - T| = 0.86$ and 0.7 K , for the second and third iterations. These results are close to the experiment made by Clark et al. (2011): these authors found that the derived temperature by this approach of heated basalt in the laboratory at 470 K was $\sim 1^\circ$ of the true measured temperature.

For the data degraded with Gaussian noise at $\text{SNR} = 100$, we found similar results to those obtained previously (Fig. 2). We observed that the temperatures of the blackbody obtained by our thermal emission correction method over the 50 spectra are very close to 'clean' spectra. For example, for the last iteration, we found an average of absolute difference between T' and $T'_{(\text{Noise})}$ over the seven temperatures of $|T' - T'_{(\text{Noise})}| = 0.22 \text{ K}$.

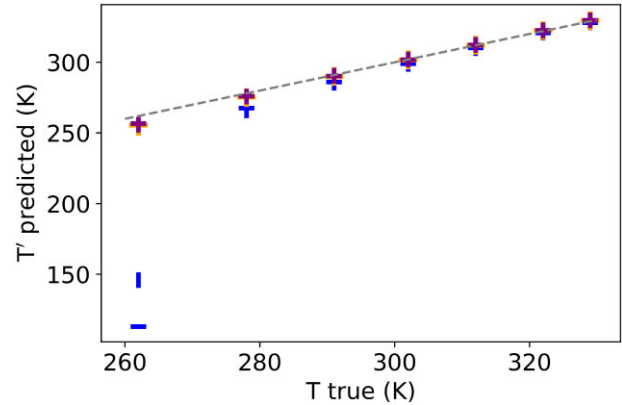


Figure 2. Plot showing the blackbody temperatures predicted by our thermal emission correction method as a function of the true temperature used to generate the data. Horizontal lines display the values obtained on 'clean' spectra, whereas vertical lines correspond to the average temperature on the 50 noisy spectra. Blue, orange, and purple symbols correspond, respectively, to the values obtained for the first, second, and third iterations. Grey line corresponds to 1:1 line.

When looking the spectra after the correction (Fig. 3), we observed that for every simulated data and every iteration, the presence of a residual thermal contribution at the edge of the spectra due to an undercorrection. This residue is nevertheless significantly reduced when the number of iterations increases. For the first iteration, the error in the thermal removal can be relatively important. For example, for the spectrum generated with a surface temperature of 329 K , we found the highest error in our simulations with an APE score equivalent to 15.94 per cent at $\lambda = 3.69 \mu\text{m}$ (Fig. 3c). However, in the same way as for temperature retrieval, the thermal correction is better for the final run of the model. Indeed, the error is significantly reduced for the third iteration, where for any wavelength, it is always limited to 5.01 per cent. In all our simulations, it is even below 2.49 per cent for wavelength lower than $3.5 \mu\text{m}$ (Figs 3c, f, and i). We noticed that expanding the number of iterations beyond three does not allow to ameliorate more the thermal correction and seems to be the limit of improvement. Overall, we found that the higher is the temperature, the larger is the error.

Emissivities retrieved by our thermal emission correction method are also overall consistent with the one used as input in the thermophysical model (ε is between 0.964 and 0.987 depending on the wavelength) to generate the data. The first iteration returns $\varepsilon \sim 0.945$ for all temperatures, whereas the second and third iterations predict emissivities within respectively 0.928 – 0.936 and 0.934 – 0.939 .

For noisy data, the model of thermal correction does not collapse although its quality is slightly degraded. For example, for the simulations at temperature $T = 262, 302,$ and 329 K , if we observed for spectra without noise that the APE scores for the final iteration at $\lambda = 3.6 \mu\text{m}$ are equivalent to respectively 3.2 per cent, 3.5 per cent, and 3.4 per cent, the noisy spectra have APE scores at the same wavelength of 3.2 per cent ($\sigma = 2.0$), 3.1 per cent ($\sigma = 2.4$), and 4.1 per cent ($\sigma = 2.7$). Here, σ corresponds to the standard deviation of the APE values over the 50 simulations. These overall similar results between noisy and 'clean' spectra indicate that the model is quite robust for this kind of simple data at MIRS' resolution.

In the second data set, which includes roughness on the simulated scene and therefore different temperatures per facet, the increased complexity of the surface compared to the first set of simulations does not strongly degrade the thermal emission correction as seen

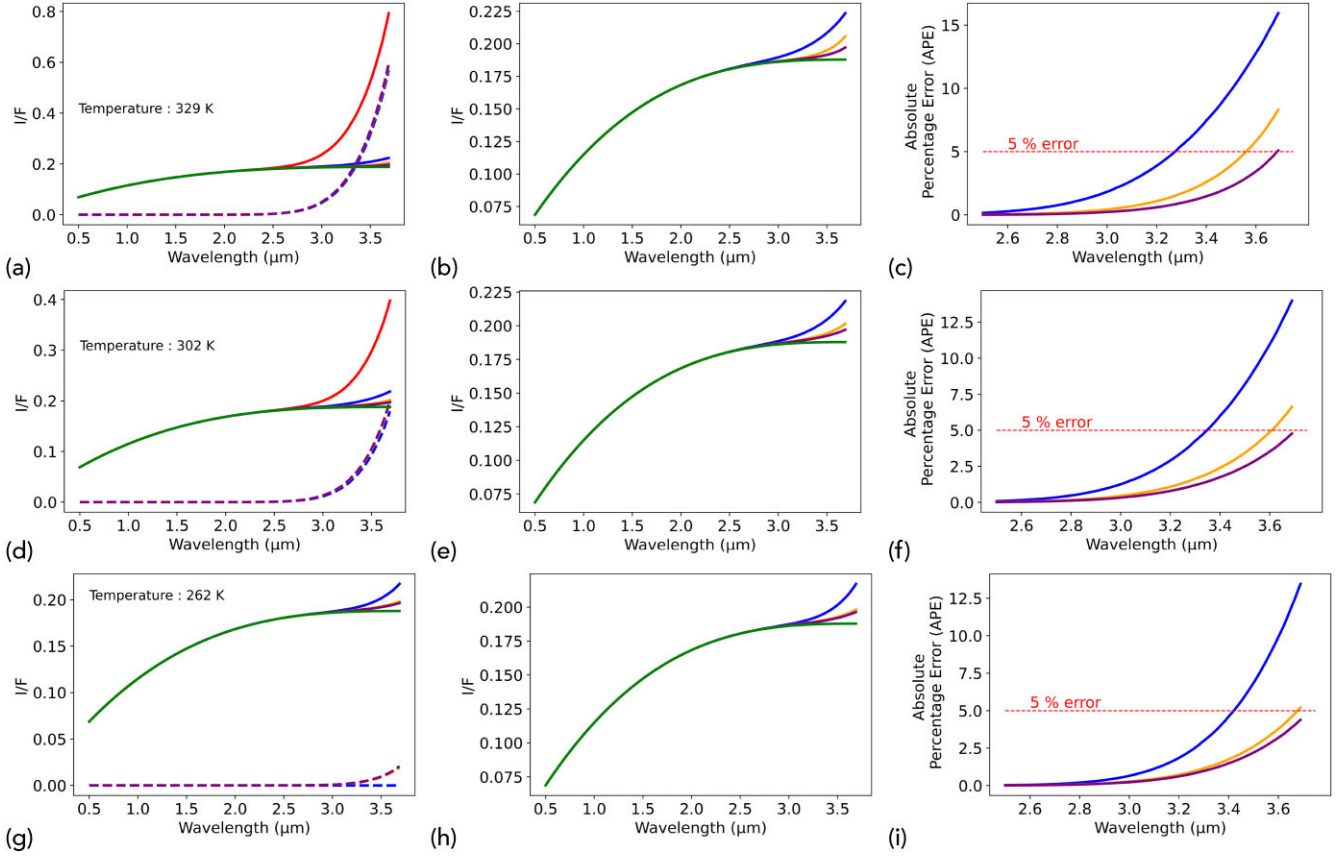


Figure 3. Test of the thermal emission correction method on the first data set of synthetic spectra, where the I/F of a flat facet with a single temperature is modelled. Different rows of plots correspond to different facet temperatures (maximum: 329 K, minimum: 262 K, and intermediate: 302 K) as simulated by means of the thermophysical model. The first column shows the synthetic I/F including the thermal contribution (red line), the reference synthetic I/F without the thermal contribution (green line), the I/F after removal of the thermal contribution by the method presented here after the first (blue line), the second (orange) and third iteration (purple); and the dashed curves represent blackbody radiation functions at the temperatures estimated from the synthetic data at the different iterations (colour-coded as before). These functions are subtracted from the original synthetic I/F to obtain the thermal emission corrected I/F . The middle column shows a zoomed-in version of the corrected spectra (colour-coded as before). The right column displays the APE value between the different thermal emission-corrected I/F spectra and the original simulated I/F without the thermal emission.

in Fig. 4, except for the first iteration. For all our data, a rise in reflectance can still be observed after the thermal correction at the red edge of the spectra similarly to previous simulations. Moreover, between high and low thermal contributions, the strongest divergence is noticed in term of error after correction. With the first iteration, we recorded an overestimation of 11.8 per cent for the corrected spectrum containing the lowest thermal contribution (at $\lambda = 3.69 \mu\text{m}$). The error rises to 16.73 per cent for the spectrum with the highest thermal contribution at the same wavelength (Fig. 4). This difference in our results indicates that for the long wavelengths of MIRS spectra corrected with only one iteration, two observations acquired on two different scenes with distinct surface temperatures, due for example to observations at different times of the day, the thermal correction can lead to produce two very different outputs, even if their composition and physical properties are rigorously similar.

Conversely, with the third iteration, the errors in the thermal corrected spectra are slightly higher than for the first data set but still remain at an acceptable level. For the final iteration, the maximum error observed is 8.1 per cent at $\lambda = 3.69 \mu\text{m}$ for the spectrum containing the highest thermal contribution (Fig. 4c). However, the error decreases quickly with decreasing wavelength and remains below 5 per cent at $\lambda < 3.35 \mu\text{m}$.

As expected, the error of the model increases with the set of noisy data similarly to the previous data set, but remains relatively low. For the highest, lowest, and intermediate thermal contributions, we found on average over the 50 simulations, respectively, APE values at $\lambda = 3.6 \mu\text{m}$ of 3.3 per cent ($\sigma = 1.7$), 4.3 per cent ($\sigma = 2.5$), and 7.8 per cent ($\sigma = 4.8$). These values are comparable to the result of the noise-free spectra, for which we observed APE values of 3.2 per cent, 4.4 per cent, and 7.2 per cent at the same wavelength.

The errors of the corrected spectra, which remain acceptable in all our simulation when using the iterative approach, is an interesting result, because it indicates that using an iterative single blackbody function to perform the thermal emission correction of MIRS simulated spectra may be suitable even for a scene containing several facets with various temperatures.

For every spectrum explored in this data set, emissivities retrieved by the model only showed minor changes. Emissivities are still equivalent to $\varepsilon \sim 0.945$ for the first iteration, and in the range 0.928–0.937 and 0.932–0.939 for the two other iterations depending on the wavelength. These values are close to the reference one and are similar to the emissivity values retrieved by our thermal emission correction method for the first data set.

In the third data set, where synthetic spectra contain an absorption band centred at $3.2 \mu\text{m}$, the thermal emission correction method

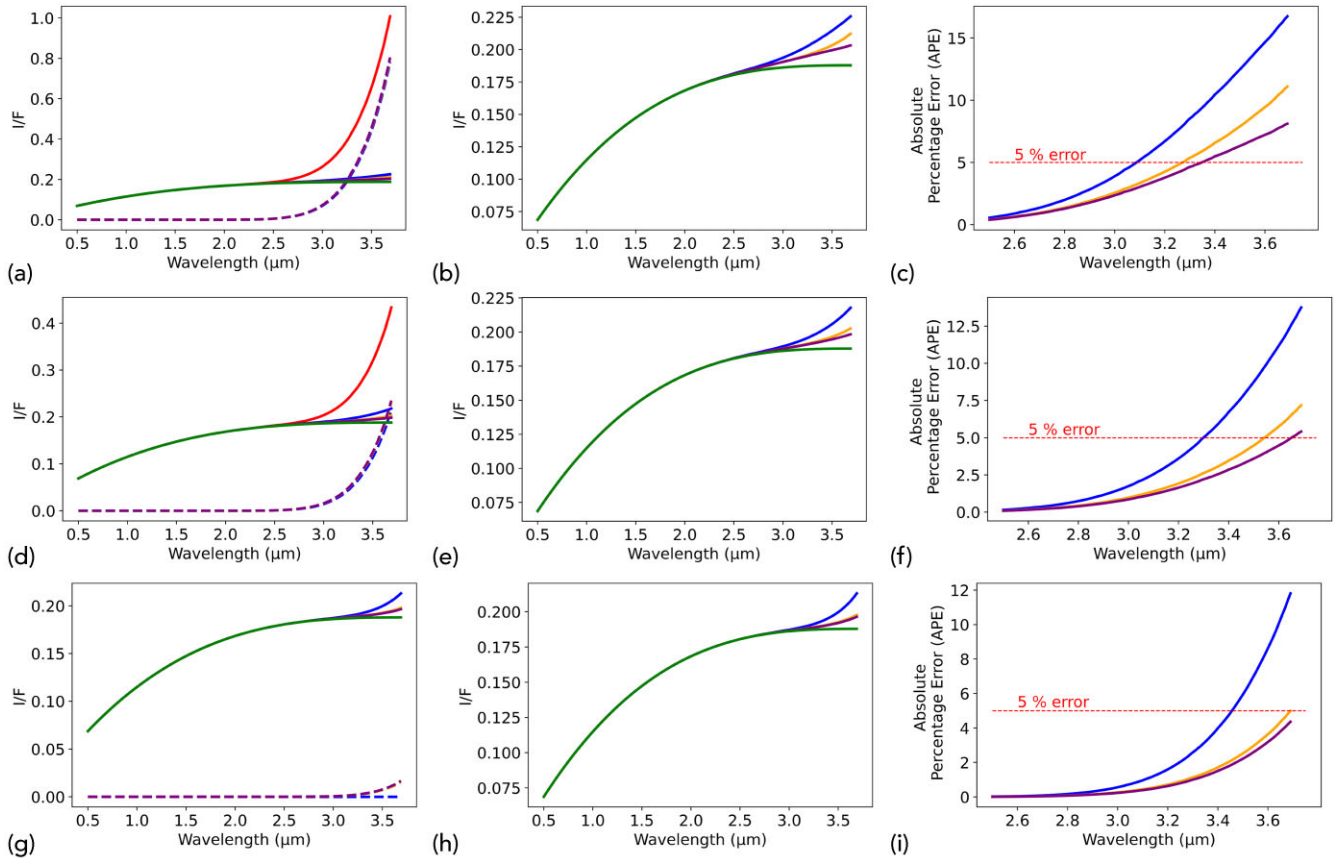


Figure 4. Test of the thermal emission correction method on the second data set of synthetic spectra, where the I/F of a flat facet with roughness represented by a surface density of hemispherical craters is modelled. Curve colours as in Fig. 2.

appears to be still efficient (Fig. 5). The third iteration gives better results for all spectra as expected, with the lowest error over the entire spectra. The general trend for data sets 1, 2, and 3, to improve each time the APE scores with the second and then the third iteration of the data treatment confirmed the efficiency of the iterative approach. For the spectrum with the highest thermal contribution, the averages APE scores over the entire spectra are equivalent for the second and third iterations to, respectively, 1.46 per cent and 0.64 per cent. We noticed a very good thermal correction near the position of the absorption band (Fig. 5c) for the second ($APE_{3.2\mu\text{m}} = 0.8$ per cent) and the third iteration ($APE_{3.2\mu\text{m}} = 0.1$ per cent). In both iterations, the shape of the $3.2\mu\text{m}$ absorption is preserved, and is only slightly overestimated. For the third iteration, the worst correction at the position of the absorption band is observed for the lowest thermal contribution, with $APE_{3.2\mu\text{m}}$ equivalent to 0.68 per cent.

Over the entire spectrum, we found with the last iteration errors in these data that are for all simulations lower than 4.02 per cent.

When we introduce noise into this spectrum, errors are in the same order as errors computed on the ‘clean’ data. The band depth is also overestimated on average over the 50 simulations of 1.6 per cent ($\sigma = 1.15$) at $\lambda = 3.2\mu\text{m}$ for the highest thermal contribution, meaning here that the noise has limited impact on the correction result. An example of noisy spectra is shown in Appendix A1. For spectra with low and intermediate thermal contribution, noisy spectra are also similarly corrected than ‘clean’ data. For the final iteration, errors at $3.2\mu\text{m}$ are, respectively, equivalent to 0.76 per cent ($\sigma = 0.6$) and 1.0 per cent ($\sigma = 0.8$). This demonstrated that the model is robust even for spectra with a level of noise comparable to MIRS data.

Emissivities estimated are still overall in line with the two previous data sets and the emissivity of reference ($\varepsilon_{\text{iteration1}} \sim 0.945$, $\varepsilon_{\text{iteration2}}$ within 0.928 and 0.937, and $\varepsilon_{\text{iteration3}}$ within 0.935 and 0.939). However, for the second and third iterations, emissivities predicted by the model will be affected by the presence of the absorption band at $3.2\mu\text{m}$. Nevertheless, this effect does not seem to have a significant impact on the thermal correction as demonstrated by overall good APE scores at this wavelength on most of our data. In all our simulations, the prediction of emissivity by the thermal correction model diverges by only 3.0 per cent with the emissivity injected into the thermophysical model in our worst case (found at $\lambda = 3.69\mu\text{m}$). On average over the entire spectrum, the error is even limited to 2.16 per cent if we consider all wavelengths. The good consistency between true emissivity and predicted emissivity shows that the Kirchhoff approximation made in the thermal correction method can be used as it only produces only limited error.

Finally, with the last data set, we studied the effect of the cosine angle correction of the thermal correction model for different geometries (i.e. 20° , 40° , 60° , and 80° of solar incidence angles).

Among all our four spectra, the one generated with a solar incidence angle of 40° without correction has the largest average error recorded for the final output of the model. For the third iteration, the mean APE value is equivalent to 1.51 per cent (with a maximum of 4.37 per cent observed at $\lambda = 3.69\mu\text{m}$). However, applying the incidence angle correction improves only slightly the result, as we then found mean APE value of 1.45 per cent (and 4.17 per cent at $3.69\mu\text{m}$). The error is slightly higher when the model is run on

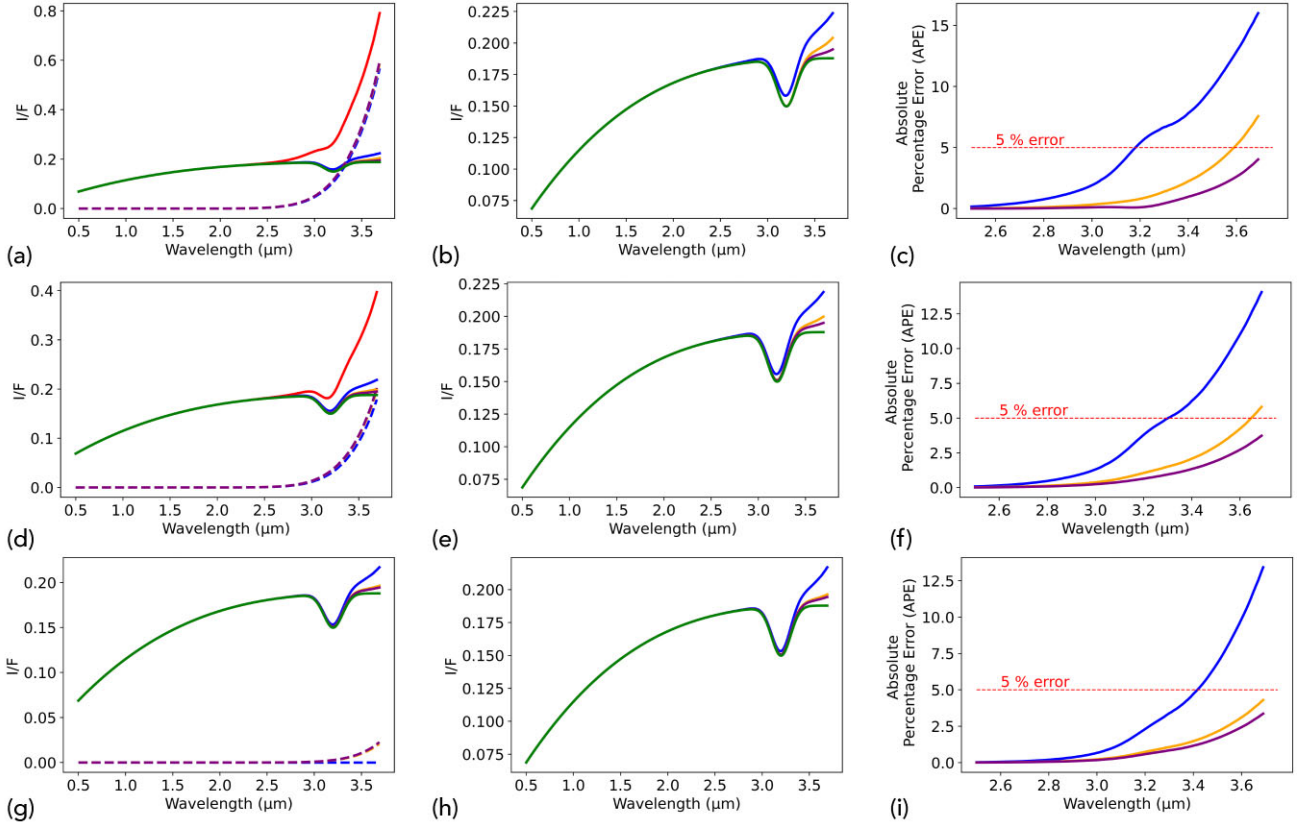


Figure 5. Test of the thermal emission correction method on the third data set of synthetic spectra, where the I/F of a flat facet with an absorption band centred at $3.2 \mu\text{m}$ is modelled. For subplot ‘g’, thermal emission is overplotted with the result from iteration 1. Curve colours as in Fig. 2.

Table 1. Mean APE (from 2.5 to $3.6 \mu\text{m}$) obtained after thermal correction for the fourth synthetic data set, with and without incidence angle correction. Mean APE at $3.69 \mu\text{m}$ are also displayed.

Incidence angle	Third iteration uncorrected (average error)	Third iteration corrected (average error)
20°	1.32	1.29
40°	1.51	1.45
60°	1.20	1.16
80°	0.74	0.74
	Third iteration uncorrected (error at $3.69 \mu\text{m}$)	Third iteration corrected (error at $3.69 \mu\text{m}$)
20°	4.53	4.46
40°	4.37	4.17
60°	3.79	3.63
80°	3.30	3.27

noisy data, but remains comparable, with an average APE value of 2.7 per cent ($\sigma = 0.5$) over the entire spectra.

For all data with different incidence angle, we found similar results as seen in Table 1, which shows the mean APE from 2.5 to $3.69 \mu\text{m}$, with and without incidence angle correction. We observed that this correction has always a minimal influence on the results. This step enables to reduce the error after the thermal correction but to a negligible extent. For all θ values (i.e. 20° , 40° , 60° , and 80°), by introducing incidence angle correction, we reduced the APE scores to a maximum of only 4.1 per cent for the third iteration.

3.2 CRISM data thermal correction

In a second step, the method of thermal correction was applied to representative spectra of the red and the blue units on Phobos using the CRISM data. We first estimated the surface temperatures. We found a range of retrieved brightness temperatures by the model on Phobos spectra within those used in our previous simulated data. On average the temperature from the blue unit is higher than the one observed in the red unit, with, respectively, 330.7 K ($\sigma = 2.0$) and 307.1 K ($\sigma = 1.7$). Due to the higher albedo of the blue region (Rivkin et al. 2002; Fraeman et al. 2012), we could expect to have a lower temperature in the blue unit compared to the red one. However, this difference is not explained by the different soil properties but rather by the fact that both units are geographically distinct, and in our data, the sunlights emerging from the terrains of the blue unit have lower incidence angles, which is among the main parameters controlling the surface temperature. We found that the blue unit has on average $\theta = 50.4^\circ \pm 4.7$ against $\theta = 63.6^\circ \pm 3.5$ for the red unit.

Regarding the emissivity predicted by the model, we found on average $\varepsilon = 0.96$ for the blue unit (i.e. all the wavelengths are averaged from 1.02 to $3.6 \mu\text{m}$) with minimum and maximum values found at a certain wavelength of 0.89 and 0.98 ; whereas the red unit displays an ε value of 0.96 with extreme values of 0.92 and 0.99 . These results are slightly higher than the emissivity suggested to model the Phobos surface by previous works (e.g. $\varepsilon = 0.9$ in Takir et al. 2022).

Although difficult to affirm with high confidence without references, at first sight, the representative spectra of the red and blue units seem to be both quite well corrected from the thermal contribution

(Figs 6a and b). At first order, we did not observe any suspicious rise or fall in reflectance at wavelength higher than $\sim 2.5 \mu\text{m}$ meaning that the method looks reliable with a satisfactory removal of the thermal contribution.

From these thermally corrected spectra, we confirm the finding made by Fraeman et al. (2014) who identified an absorption band centred at $\sim 2.8 \mu\text{m}$. This spectral feature is thought to be associated with hydroxylated materials and possibly linked to the presence of structural OH- in a desiccated phyllosilicate such as non-tronite, or by OH- formed by exogenic space weathering processing. Unfortunately, CRISM data around $2.75 \mu\text{m}$ are compromised by a boundary between filters mounted to the IR detector that blocks higher orders from the diffraction grating leading to a gap in the spectra. Consequently, it is not straightforward to identify with great confidence the exact wavelength at which the absorption minimum occurs. After the thermal correction of CRISM data, we observed for both the red and blue units a sharp decrease of the absolute reflectance between 2.7 and $2.8 \mu\text{m}$ (corresponding overall to the two edges of the gap in the spectra), which confirms the presence of an absorption band (Fig. 6). If this absorption could already be perceived without thermal correction for the averaged spectrum of the red unit (due to the lower surface temperatures and so lower thermal contribution), it was more tricky for the averaged spectrum of the blue unit (Figs 6a and b, black spectra). When looking for individual spectrum in our data set, we found unfortunately no obvious correlation between the strength of the $2.8 \mu\text{m}$ absorption and the slope of the spectrum. On average, the red unit appears to have a slightly deeper absorption at this wavelength than the blue unit. The depth of the bands compared to the shoulders are respectively equivalent to 0.077 ($\sigma = 0.014$) and 0.055 ($\sigma = 0.018$). It is thought that the blue unit mineralogy could represent a less mature version of the red unit mineralogy, or a different mineralogy altogether (Rivkin et al. 2002). Variations in the depth of the $2.8 \mu\text{m}$ absorption across the surface of Phobos could reflect this difference in mineralogy, or difference in the degree of space weathering, or a combination of the two Fraeman et al. (2014).

Further into the IR, an apparent absorption is also noticed in the thermally corrected CRISM spectra at $3.2 \mu\text{m}$ in both units. Smaller absorptions are also present at 3.45 and $3.62 \mu\text{m}$ in the blue unit. While this feature at $3.2 \mu\text{m}$ appears stronger in our restricted CRISM data representative of the blue unit compared to the red unit (with respectively, band depths of 0.17 ± 0.04 and 0.04 ± 0.03), no correlation at the scale of the entire surface of Phobos is observed between the VNIR ratio and band depth. Furthermore, band depth map of this $3.2 \mu\text{m}$ feature shows it has a columnar dependence (Fig. 6e) and no any obvious association with geological features, which would be expected if it was a true absorption. Consequently, the apparent $3.2 \mu\text{m}$ absorption is likely an artefact, as there is a known issue in the radiometric calibration of the instrument near $3.18 \mu\text{m}$ due to the zone 1 and 2 filter boundaries (Murchie et al. 2009). Moreover, although our simulations on synthetic data have shown that the model of thermal tail removal may have some errors at these longer wavelengths, an incorrect thermal subtraction is unable to produce the absorption bands observed on CRISM data, because it could only produce a constant steep downward or upward slope.

Even though, the most convincing explanation is that this feature is an artefact, it should be investigated by MIRS in the future because if its origin is linked to the composition of Phobos (e.g. due to the presence of organic materials), it could have important implications for understanding the history of the formation and evolution of the Martian satellite. Indeed, similar absorption at or near $3.2 \mu\text{m}$ was observed in other small bodies of the Solar system and even possibly in Phobos and Deimos by other instruments. For example, based on

telescopic observations of Phobos with the NASA Infrared Telescope Facility (IRTF), a possible absorption band could be present in the red unit around $3.1 \mu\text{m}$ (Rivkin et al. 2002) that could be also present in Deimos surface, although the noise is relatively high in the IRTF data, which give only low confidence in this identification.

Both absorption around 2.8 and $3.2 \mu\text{m}$ were also observed in several small bodies such as asteroids or comets. For instance, many observations of the large C/P spectroscopic types (Tholen classification, Tholen 1984) asteroid Bamberg have shown in several observations an absorption band centres near or at $3.2 \mu\text{m}$, small absorption near $2.9 \mu\text{m}$, as well as at $3.6 \mu\text{m}$ (Rivkin, Howell & Emery 2019). Cybele asteroids, C/P/D largely primitive asteroids (Barucci et al. 1987), situated between the main-belt and Jupiter Trojan asteroids shown also an absorption at $3.2 \mu\text{m}$ (Hargrove et al. 2012). Otherwise, Europa, Euphrosyne, and Patientia, respectively, C/F, C, and C/U-class asteroids exhibit a band centred at $\sim 3.15 \mu\text{m}$ (Takir & Emery 2012). These features observed in these low-density and low-albedo asteroids could be related to those observed in CRISM data, although the band is slightly shifted compared to our observations. Cybele and Euphrosyne asteroids also exhibit an absorption at $0.65 \mu\text{m}$ that is similar to the feature observed on Martian moons (Fraeman et al. 2014). In addition, the surface of the comet 67P/Churyumov–Gerasimenko also shows some similarities with CRISM observation of Phobos. The VIRTIS-M (Visible and Infrared Thermal Imaging Spectrometer) instrument recorded spectra that were almost uniform with very low reflectance, positive visible and IR spectral slopes, as well as a broad absorption feature from 2.8 to $3.6 \mu\text{m}$, centred at $3.2 \mu\text{m}$, thought to be due to the presence of several species such as organic materials (e.g. ammonium salts) possibly combined with water ice (Capaccioni et al. 2015; Poch et al. 2020).

Although CRISM calibration effect is a possibility to be at the origin or to influence the $3.2 \mu\text{m}$ absorption observed, new data are needed and will be essential to definitively validate or not this assumption, given that the presence of a true absorption would have important consequences for our understanding of the materials that make up the Phobos surface and its history. Additional data with no gap in the spectra are also required as well to study the exact position of the absorption band near $2.8 \mu\text{m}$. In the near future, MMX Japan's upcoming mission will provide with MIRS new IR spectroscopy analyses of the Martian moon surfaces and will help to decipher their formation and evolution mechanisms.

4 CONCLUSION

In this study, we applied the method of thermal emission correction for IR spectroscopy analyses developed by (Clark et al. 2011) with the aim of determining the efficiency of this correction and its possible application for future MIRS observations of Phobos and Deimos. The simple method, based on *Planck* body fit was first used to correct the thermal tail of synthetic spectra of Phobos, generated by means of a thermophysical model (Delbo et al. 2015). Several spectral data sets corresponding to the observation of different scenes including various temperatures, roughness, the presence of synthetic absorption bands, or photometric angles were generated and corrected.

Our results show that this simple method gives at first order relatively good results despite undercorrections are observed in all our simulations leading to a small rise of the reflectance at the red edge of the spectra. The model is iterative, and we observed that such an approach significantly improves the thermal tail correction compared with using a single continuum extrapolation and a blackbody fit. We quantified the error on the thermal tail corrected spectra. Based on

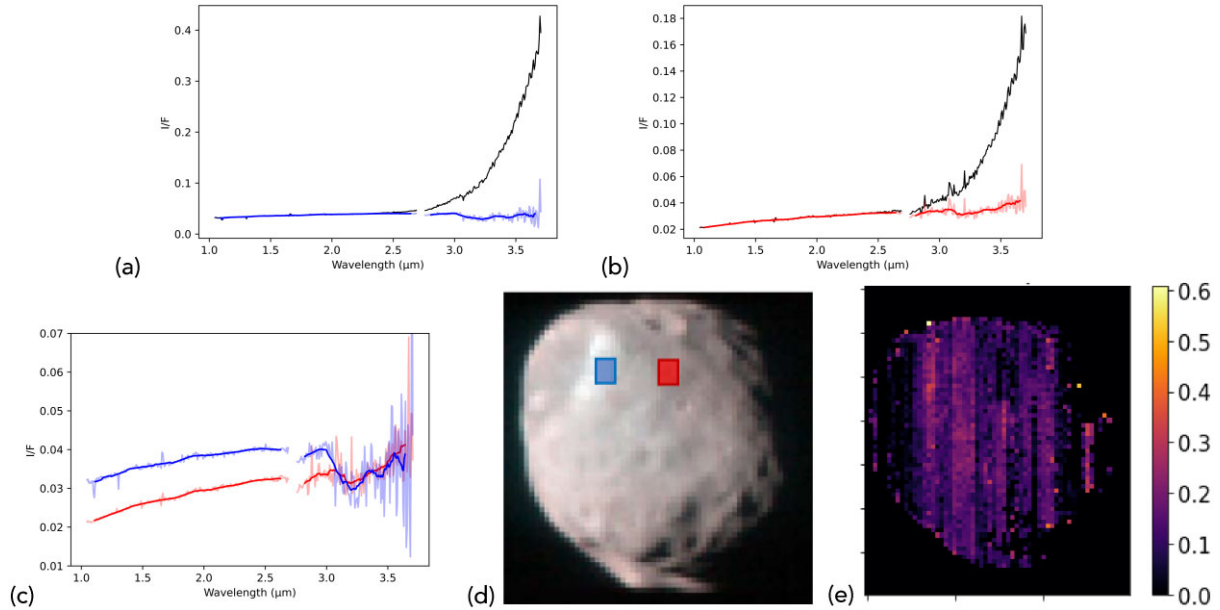


Figure 6. Representative CRISM I/F spectra from Phobos blue (a) and red (b) units. Black lines display spectra without the removal of the thermal emission. To reduce noise in the data, the 12 spectra of the blue and red units were merged, respectively, in order to obtain only two spectra representative of the two units (faint lines), and smoothed using a mean filter with a width of 20 channels (heavy lines). (c) Layering of the blue and red units corrected spectra. (d) Localization of the blue and red unit spectra that were used in this study. (e) Band depth map of the $3.2\ \mu\text{m}$ absorption at the surface of Phobos, which is likely an artefact of the CRISM radiometric calibration.

all our simulations, we found for the third and final iterations of the model that this error is always under 8.1 per cent on the continuum of the spectra at any wavelength. In most of our simulations, the error is even significantly below this value for wavelengths lower than $3.5\ \mu\text{m}$. Consequently, we found good results of the method in the most useful part of the IR spectrum, where the signature of several species could be observed such as hydrated silicate minerals (feature at $2.7\text{--}2.8\ \mu\text{m}$), water ice (absorption band around $3.0\ \mu\text{m}$) or organic materials ($3.2\text{--}3.5\ \mu\text{m}$). We investigated the result of the method when an absorption band is located in the emission-contaminated part of spectra. We found that the model is still robust and still gives good outcomes for the correction of the entire spectrum. If the strength of the absorption band is preserved in most cases, it can be sometimes overestimated by an order of magnitude of a few per cent. As the error produced by the model is smooth and mostly on the slope, this means that the centre of potential bands could be retrieved with good accuracy.

To be as close to MIRS data as possible, we also introduced Gaussian noise into our simulated spectra ($\text{SNR} = 100$). We observed that the model does not collapse, and if the error in the correction in some cases slightly increases, it remains minor and comparable to ‘clean’ spectra.

From this thermal correction method, we conclude that we can be confident to correct the thermal tail of future MIRS data (and other IR spectral data) in the spectral range of $0.9\text{--}3.5\ \mu\text{m}$. The method is suitable for future MIRS observations and could be used at least during the early stage of the MMX mission, for which shape model of the Martian moons with sufficient spatial resolution will be available yet, which makes it impossible to use more sophisticated methods (e.g. modelling using photometric functions). Although simplistic, this empirical thermal correction can be used to make a first quick analysis and interpretation of the IR data obtained by MIRS.

Application of the model of thermal correction to CRISM observations of Phobos confirms, at first sight, the good efficiency of the method. By studying representative spectra of the blue and red units of Phobos we confirmed the result from the work made by Fraeman et al. (2014) and the presence of an absorption band centred near $2.8\ \mu\text{m}$ linked to hydroxylated materials. From these data, we also noticed an additional strong apparent absorption at $3.2\ \mu\text{m}$, which origin remains uncertain, at this stage. If a calibration artefact on CRISM data could be a reasonable assumption and cannot be discarded, additional observations are required to definitively confirm this hypothesis. In the coming years, the new analyses made by MIRS with high spatial and spectral resolutions will be an asset to study in depth the spectral properties of the Martian moon surfaces and better constrain their formation processes. The good spectral and spatial resolutions of MIRS and the absence of gap in the spectra and radiometric calibration artefact in the $3.2\ \mu\text{m}$ spectral range will enable us to study these signatures. If such a finding is established, due for example to the presence of organic compounds, the similar spectral signature between Phobos and some asteroids will be an argument in favour of the capture scenario as the origin of the moon, and/or it will suggest that they share a common history and potentially that Phobos underwent similar alteration processes than other small bodies of the Solar system.

ACKNOWLEDGEMENTS

This study was carried out in support of the MIRS instrument found by Centre National d’Etudes Spatiales in France. AAF was supported by the National Aeronautics and Space Administration (NASA) MMX (Martian Moons Exploration) Participating Scientist Program, and her research was carried out at the Jet Propulsion Laboratory, California Institute of Technology, under a contract with the NASA (80NM0018D0004).

DATA AVAILABILITY

The data underlying this article will be shared on reasonable request to the corresponding author.

REFERENCES

- Barucci M. A., Capria M. T., Coradini A., Fulchignoni M., 1987, *Icarus*, 72, 304
- Barucci M. A. et al., 2021, *Earth Planets Space*, 73, 1
- Brown M. E. et al., 2021, *Planet. Sci. J.*, 2, 170
- Capaccioni F. et al., 2015, *Science*, 347, aaa0628
- Choo T. H. et al., 2014, *Acta Astron.*, 93, 490
- Clark R. N., Pieters C. M., Green R. O., Boardman J., Petro N. E., 2011, *J. Geophys. Res.: Planets*, 116, E00G1
- Coradini A. et al., 2011, *Science*, 334, 492
- Craddock R. A., 2011, *Icarus*, 211, 1150
- Delbo M., Cellino A., Tedesco E., 2007, *Icarus*, 188, 266
- Delbo M., Mueller M., Emery J. P., Rozitis B., Capria M. T., 2015, *Asteroids IV*, 1, 107
- DellaGiustina D. et al., 2019, *Nat. Astron.*, 3, 341
- Đurech J., Delbo M., Carry B., Hanuš J., Ali-Lagoa V., 2017, *A&A*, 604, A27
- Fraeman A. et al., 2012, *J. Geophys. Res.: Planets*, 117, E00J15
- Fraeman A., Murchie S., Arvidson R., Clark R., Morris R., Rivkin A., Vilas F., 2014, *Icarus*, 229, 196
- Giuranna M., Roush T., Duxbury T., Hogan R., Carli C., Geminale A., Formisano V., 2011, *Planet. Space Sci.*, 59, 1308
- Hamilton V. et al., 2019, *Nat. Astron.*, 3, 332
- Hapke B., 1984, *Icarus*, 59, 41
- Hapke B., 1986, *Icarus*, 67, 264
- Hapke B., 1993, *Theory of Reflectance and Emittance Spectroscopy*. Cambridge University Press, Cambridge, UK
- Hapke B., 2012, *Theory of Reflectance and Emittance Spectroscopy*, 2nd edn. Cambridge University Press, Cambridge, UK
- Hapke B., Wells E., 1981, *J. Geophys. Res.: Solid Earth*, 86, 3055
- Hargrove K. D., Kelley M. S., Campins H., Licandro J., Emery J., 2012, *Icarus*, 221, 453
- Hartmann W. K., 1990, *Icarus*, 87, 236
- Hesselbrock A. J., Minton D. A., 2017, *Nat. Geosci.*, 10, 266
- Higuchi A., Ida S., 2017, *AJ*, 153, 155
- Hyodo R., Genda H., Charnoz S., Pignatale F. C., Rosenblatt P., 2018, *ApJ*, 860, 150
- Jacobson R., 2010, *AJ*, 139, 668
- Kuramoto K. et al., 2022 *Earth Planets Space*, 74, 1
- Kurucz R., 1993, Cambridge, Mass.: Smithsonian Astrophysical Observatory, Robert Kurucz CD-ROM No. 13
- Li S., Milliken R. E., 2016, *J. Geophys. Res.: Planets*, 121, 2081
- Li F., Yuan Y., Fu Y., Chen J., 2023, *AJ*, 166, 93
- Lynch D. K. et al., 2007, *AJ*, 134, 1459
- Marchis F. et al., 2012, *Icarus*, 221, 1130
- Mermly G. C., Schmidt F., Andrieu F., Cornet T., Belgacem I., Altobelli N., 2023, *Icarus*, 394, 115379
- Murchie S., Erard S., 1996, *Icarus*, 123, 63
- Murchie S. L. et al., 1991, *J. Geophys. Res.: Solid Earth*, 96, 5925
- Murchie S. L. et al., 2009, *J. Geophys. Res.: Planets*, 114, E00D07
- Poch O. et al., 2020, *Science*, 367, eaaw7462
- Poggiali G. et al., 2022, *MNRAS*, 516, 465
- Raponi A. et al., 2019, *Icarus*, 320, 83
- Rivkin A., Brown R., Trilling D., Bell Iii J., Plassmann J., 2002, *Icarus*, 156, 64
- Rivkin A. S., Howell E. S., Emery J. P., 2019, *J. Geophys. Res.: Planets*, 124, 1393
- Ronnet T., Vernazza P., Mousis O., Brugger B., Beck P., Devouard B., Witasse O., Cipriani F., 2016, *ApJ*, 828, 109
- Rosenblatt P., 2011, *A&AR*, 19, 1
- Rosenblatt P., Charnoz S., 2012, *Icarus*, 221, 806
- Rosenblatt P., Charnoz S., Dunseath K. M., Terao-Dunseath M., Trinh A., Hyodo R., Genda H., Toupin S., 2016, *Nat. Geosci.*, 9, 581
- Simon A. A. et al., 2020, *Science*, 370, eabc3522
- Stansberry J. et al., 2012, *Icarus*, 219, 676
- Takir D., Emery J. P., 2012, *Icarus*, 219, 641
- Takir D., Matsuoka M., Waiters A., Kaluna H., Usui T., 2022, *Icarus*, 371, 114691
- Tholen D. J., 1984, *Asteroid Taxonomy from Cluster Analysis of Photometry*. University of Arizona, Tucson, AZ
- Thomas P., 1993, *Icarus*, 105, 326
- Tosi F. et al., 2014, *Icarus*, 240, 36
- Willner K., Shi X., Oberst J., 2014, *Planet. Space Sci.*, 102, 51

APPENDIX A: SOME EXTRA MATERIAL

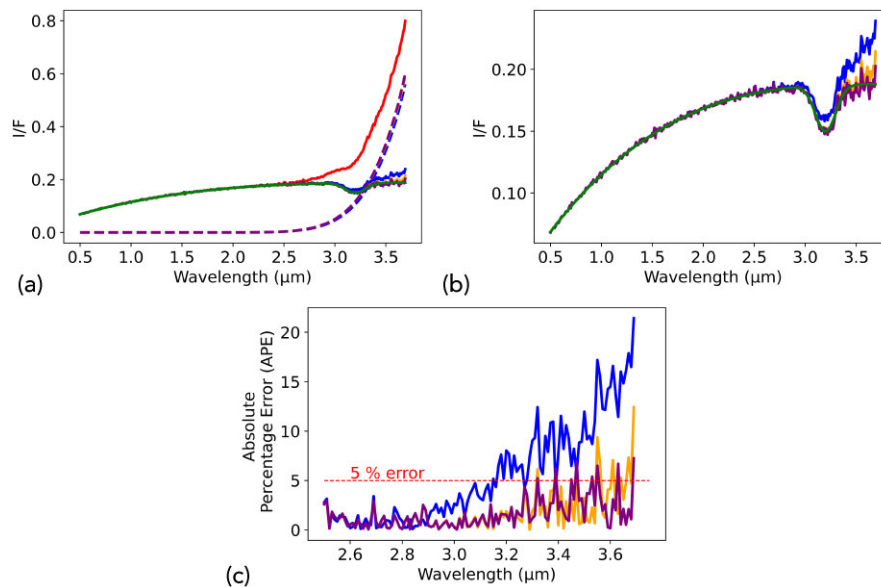


Figure A1. Example of introduction of Gaussian noise into our simulated spectra for the third data set (highest thermal contribution). (a) Synthetic I/F including the thermal contribution (red line), the reference synthetic I/F without the thermal contribution (green line), the I/F after removal of the thermal contribution by the method presented here after the first (blue line), the second (orange line), and third iteration (purple line); the dashed curves represent blackbody radiation functions at the temperatures estimated from the synthetic data at the different iterations (colour-coded as before). These functions are subtracted from the original synthetic I/F to obtain the thermal emission corrected I/F . (b) Zoomed-in version of the corrected spectra (colour-coded as before). (c) APE value between the different thermal emission-corrected I/F spectra and the original simulated I/F without the thermal emission.

This paper has been typeset from a $\text{\TeX}/\text{\LaTeX}$ file prepared by the author.